Experimental Validation of a Plane Wave Generator for Low Frequency Applications

F. Saccardi[1], FELLOW AMTA, V. Schirosi[1], A. Giacomini[1], SENIOR AMTA, Jaydeep Singh[1], L. Foged[1], FELLOW AMTA, N. Gross[1], E. Kaverine[1] E. Szpindor[1], T. McKeown[1]
(1) MVG, MICROWAVE VISION GROUP

***Abstract*— Plane Wave Generators (PWGs) utilize arrays of radiating elements to approximate plane wavefronts, thereby creating localized far-field-like conditions within a Quiet Zone (QZ). Their compact form factor makes them especially advantageous at low frequencies, such as in the VHF and UHF bands, where traditional Compact Antenna Test Ranges (CATRs) become impractically large. This paper presents results from a comprehensive validation campaign of a 19-element PWG demonstrator, conducted as part of a broader development program aimed at realizing a full-scale system for VHF/UHF testing. The campaign, executed at Pulsaart by AGC, involved both element-level and array-level assessments using a spherical near-field multi-probe system. Key objectives included validating QZ synthesis, calibrating array excitations via digital twin modeling and field expansion methods, and quantifying realized excitation errors. The findings confirm the robustness of the PWG design, the effectiveness of the calibration process, and the minimal impact of mutual coupling and active impedance variations on performance.**

***Index Terms*— far field, low frequency, multi-probe, plane wave generator, system level testing, uhf, vhf.**

I. INTRODUCTION

Plane Wave Generators (PWGs) are specialized antenna test systems designed to recreate far-field conditions within a confined region known as the Quiet Zone (QZ), like what can be obtained by more widely known Compact Antenna Test Range (CATR) techniques [1]-[5]. This is accomplished by strategically arranging and exciting an array of radiating elements so that their combined output approximates a uniform amplitude and phase front, i.e., a plane wave within the QZ even though it is clearly situated in the near-field region of the array. At lower frequencies, PWGs can often outperform similarly sized CATRs in approximating far-field behavior, as CATRs require significantly larger physical dimensions to achieve comparable performance.

Advancements in design and implementation have transformed PWGs from a theoretical concept into a practical tool used in diverse electromagnetic testing environments. Today, they support measurements of both passive and active antennas across a wide frequency range, from VHF/UHF [5]-[6] up to the millimeter-wave domain where the PWG agility of movement makes it a superior choice for some testing scenarios [4]. However, one of the key limitations of PWGs lies in the discrete spatial sampling of the aperture by the radiating elements. This constraint limits the maximum achievable electrical size of the QZ, confining practical usage to cases where PWG-specific advantages, such as reduced size, are most beneficial. A prominent example is in low-frequency applications (e.g., VHF and UHF), where compactness is a critical design driver. In such scenarios, PWGs are increasingly viewed as complementary to traditional CATR systems, and under specific constraints, can even serve as viable alternatives.

To accurately emulate far-field conditions within the QZ, precise control of the excitation at each array element, both amplitude and phase, is essential. Even small deviations could distort the uniformity of the synthesized wavefront. To address this, effective calibration techniques must be employed to correct various sources of error, including imperfections in the distributions network, amplitude and phase errors in the beamforming network, cable length mismatches, element variability, and mutual coupling effects.

This paper investigates the criticality of such deviations on practical PWG designs aiming at minimizing excitation errors in the final design stage. The study is based on a 19-element sub-array, serving as a demonstrator within a larger PWG system currently under development.

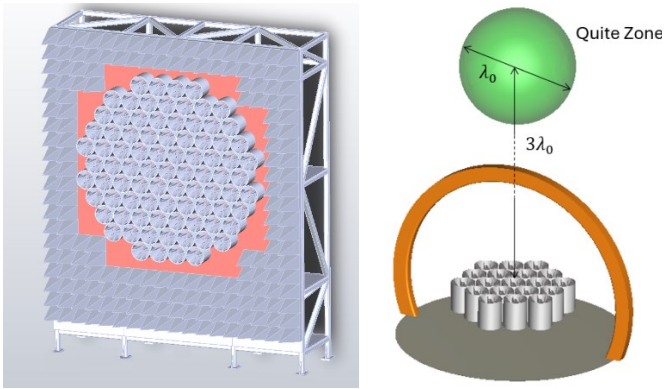

Figure 1: Full PWG array solution for measurements of wide band antennas and active decives at VHF/UHF frequencies (left). Skecth showing the investigated 19-element PWG sub-array measured in the Pulsart by AGC spherical near field automotive range (right).

II. MEASURED PWG

The PWG evaluated in this study was implemented as a modular system comprising several sub-arrays, each populated with identical radiating elements. For system-level validation of this concept, a 19-element prototype sub-array, representing the core section of the intended full-scale PWG for VHF/UHF applications, was fabricated and characterized. The tested array spans approximately $2.1\lambda_0$ in diameter, with an inter-element spacing of $0.4\lambda_0$, where λ_0 corresponds to the lowest frequency in the design band (f_0). Performance was evaluated through QZ synthesis across multiple frequencies ranging from f_0 to $8f_0$, with several QZ sizes and distances analyzed. This paper primarily focuses on one configuration: a QZ with a diameter of $1\lambda_0$, located $3\lambda_0$ from the PWG aperture, as shown in Figure 1. The frequency range optimized for this setup spans from f_0 to $2f_0$.

The array elements are excited via a uniform feed network designed to deliver consistent amplitude and phase values. Equal-length, phase-matched cables are used throughout the system to minimize differential delays and ensure stable performance across a broad frequency range, supporting up to a 10:1 operational bandwidth. Amplitude and phase control for each sub-array is implemented using analog wideband modules (Beam Forming Unit, BFU) that are digitally programmable, following the methodology described in [7]. The all-analog signal path eliminates the need for analog-to-digital or digital-to-analog conversions, thereby preserving wideband signal integrity. Due to the use of linear components, the system is reciprocal and supports bi-directional operation with minimal mismatch between transmit and receive paths. Although amplification is not included in the current configuration, the architecture allows for its integration as an optional enhancement.

The programmable BFUs provide amplitude control with 0.5 dB resolution across a 0–40 dB range. Phase adjustments are handled by digitally controlled phase shifters capable of better than 2° resolution across the full operating band. Figure 2 illustrates the wideband amplitude and phase control module, along with measured phase responses from four representative units. The imposed phase, tunable from 0° to 360°, remains highly stable across the full bandwidth, with negligible frequency dependence, making the modules well suited for broadband operation. To account for any residual deviations in amplitude or phase, correction tables are derived from individual acceptance tests performed on each module.

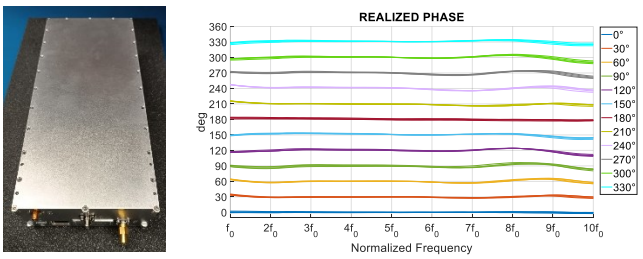

Figure 2: Wideband BFU developed for this validation (left). Measured phase response of 4 different phase shifter modules in a 10:1 bandwidth (right).

III. PWG SIMULATION USING A DIGITAL TWIN

To support the system-level performance evaluation, full-wave electromagnetic simulations were conducted to develop a high-fidelity Digital Twin (DT) of the complete PWG configuration. Besides predicting the radiated fields, this model played a central role in optimizing the amplitude and phase excitation coefficients applied to the array. One of the key objectives of this effort was to assess the accuracy of the digital twin, with the intent of using it as a reference tool for defining excitation strategies for the full-scale PWG system. A rendering of the 19-element digital twin model is provided in Figure 1 (right).

IV. VALIDATION MEASUREMENTS

Experimental validation of the PWG sub-array was performed at the Pulsaart by AGC facility in Belgium, using an MVG-developed multi-probe spherical near-field (SNF) system. This automotive-grade range, operating from approx. 70 MHz to 6 GHz, enabled wideband evaluation of the sub-array's performance. As shown in Figure 1 (right), the array was placed on the ground plane and oriented to radiate upward into the hemispherical probe system.

Despite the electrically compact size of the 19-element array, it exhibits relatively high directivity. This, combined with the upward pointing configuration, allowed the radiated fields to remain well-contained within the hemispherical measurement system, thus minimizing truncation effects and improving measurement fidelity.

The excitation coefficients applied to the Beam Forming Network (BFN) have been derived from the DT optimization. Specifically, the simulated SNF, obtained from the optimized DT (denoted as $SNF_{DT}(\boldsymbol{r}, f)$) has been expanded using (1):

$$SNF_{DT}(\boldsymbol{r}, f) = \sum_i C_{input,i}(f) SNF_i(\boldsymbol{r}, f) \qquad (1)$$

Here, the basis functions $SNF_i(\boldsymbol{r}, f)$ are obtained from measurements of each subarray (i) of the PWG. These measurements are processed using Spherical Wave Expansion (SWE) [2] to compute the SNF at the same spherical coordinates ($\boldsymbol{r}$) as the DT field. By inverting (1), the calibrated excitation coefficients ($C_{input,i}(f)$) are retrieved and used as input to the PWG. This process is repeated for each frequency (f) available in the DT, resulting in a set of coefficients per frequency. These sets are then averaged in frequency obtaining a single set of excitation coefficients.

Once the calibrated set of coefficients have been found, the array has been driven from a single input port, and SNF data of the whole PWG have been acquired over the hemispherical surface. These measurements have then been post-processed using, again, the SWE-based near-field-to-near-field (NF-to-NF) propagation techniques, allowing field extrapolation to the Quiet Zone (QZ) reference plane, as described in [4].

Measurement results were directly compared to the simulated fields generated by the digital twin. Figure 3 presents two-dimensional amplitude and phase maps along the xz-plane

at $1.5f_0$, illustrating the level of agreement between predicted and measured fields. The close correspondence validates both the excitation strategy and physical implementation of the PWG.

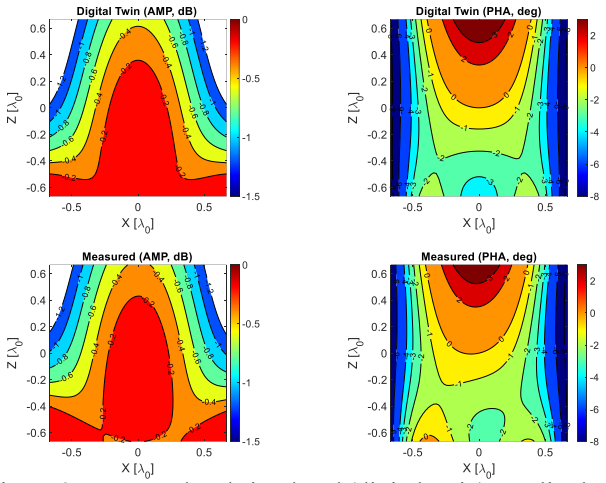

Figure 3: Measured and simulated (digital-twin) amplitude and phase field maps over the QZ down-range at $1.5f_0$ using wide-band coefficients optimized at $1f_0 - 2f_0$.

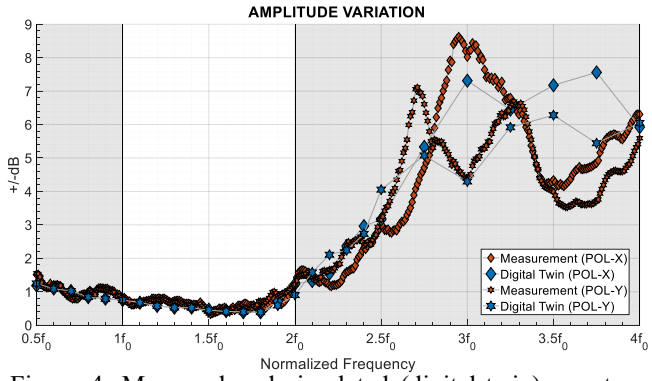

Figure 4: Measured and simulated (digital-twin) worst case (nominal-to-peak) amplitude variations over the QZ volume with wide-band optimization in the $1f_0 - 2f_0$ band.

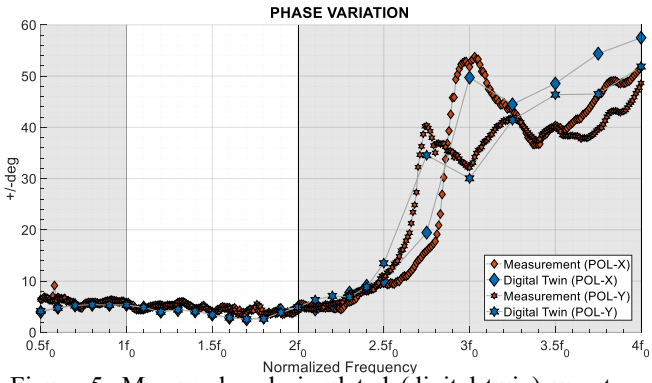

Figure 5: Measured and simulated (digital-twin) worst case (nominal-to-peak) phase variations over the QZ volume with wide-band optimization in the $1f_0 - 2f_0$ band.

Figures 4 and 5 show the nominal-to-peak amplitude and phase variations across the QZ volume for both orthogonal polarizations, based on the coefficient set optimized for the f_0 to $2f_0$ frequency band. While overall agreement between measurement and simulation is strong both inside and outside the optimized band, minor differences are noted. These can be attributed to typical uncertainties in measurement as well as residual errors in the realized excitation values.

V. Exitation Error Investigation

The error in the realized excitation coefficients of the measured array has been analyzed using a field expansion method, and the results have been compared with those obtained from conducted measurements on the individual programmable BFU.

Similar to (1), the considered field expansion method is based on equation (2) [8], [9].

$$SNF_{pwg}(\boldsymbol{r}, f) = \sum_i C_{realized,i}(f) SNF_i(\boldsymbol{r}, f) \qquad (2)$$

In this case, the SNF obtained from the measurement of the PWG excited with the calibrated coefficients ($SNF_{pwg}(\boldsymbol{r}, f)$) is projected over the same basis functions described above ($SNF_i(\boldsymbol{r}, f)$). By inverting (2) the actual realized coefficients are now obtained ($C_{realized,i}(f)$).

This approach offers the advantage of providing a reliable estimate of excitation errors introduced by the BFN, since the subarrays are individually measured. These estimates serve as a meaningful reference for comparison with the errors obtained from conducted measurements on each programmable BFU.

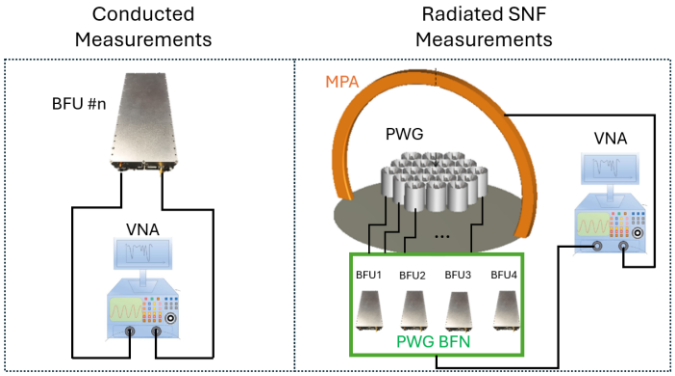

Figure 6: Illustrations of the conducted and radiated SNF measurement setups.

Below a comparison between the results obtained with the two distinct measurement setups illustrated in Figure 6 is shown.

The left-side setup represents a straightforward bench-top conducted measurement scenario, where each individual programmable BFU is characterized using a Vector Network Analyzer (VNA). In this setup, the same excitation coefficients ($C_{input,i}$) used as input to the PWG, are applied to each BFU.

For each BFU, an S_{21} measurement is performed, and the excitation error ($\varepsilon_{conducted}$), is calculated using (3):

$$\varepsilon_{conducted}(f) = \left(\frac{S_{21,i}(f)}{S_{21,ref}(f)}\right)/C_{input,i} \quad (3)$$

where $S_{21,ref}(f)$ is the reference measurement corresponding to the "0 dB, 0°" state, common to all BFUs.

The right-side setup in Figure 6 corresponds to the SNF measurement configuration used for validating the PWG. This setup also enables verification of the realized excitation coefficients via the above-described field expansion method. Using complex values, the error between the input and realized coefficients is quantified by (4):

$$\varepsilon_{expansion}(f) = C_{realized\ i}(f)/C_{input,i} \quad (4)$$

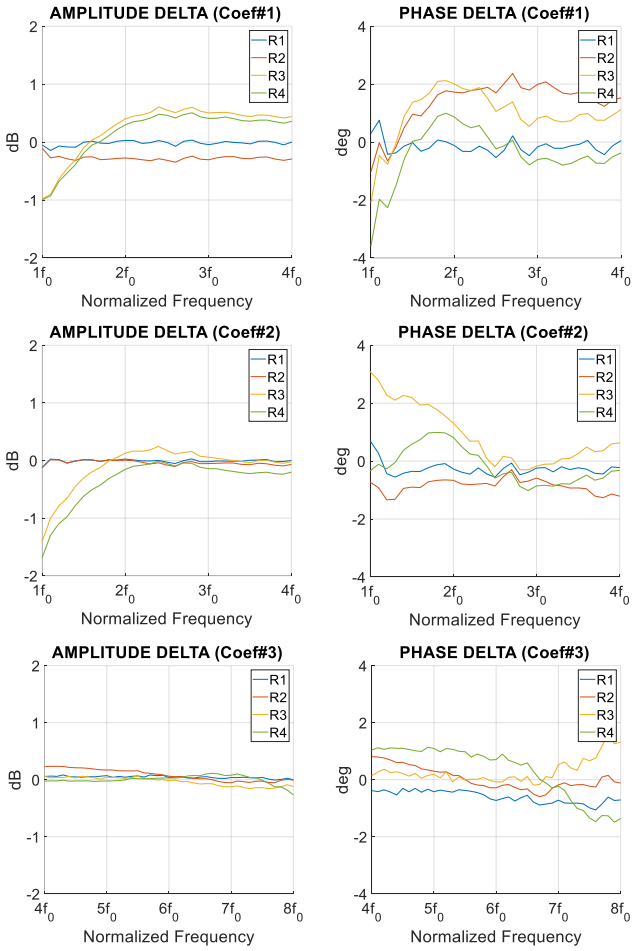

Figure 7: Difference between excitation errors measured with conducted measurement vs. radiated measurement and field expansion method.

Figure 7 presents the differences in amplitude (dB) and phase (degrees) between $\varepsilon_{conducted}$ and $\varepsilon_{expansion}$ for three synthesized QZ configurations:

- optimization in the 1f₀ - 2f₀ range (first row)
- optimization in the 2f₀ - 4f₀ range (second row)
- optimization in the 4f₀ - 8f₀ range (third row)

For the first two configurations, results are shown over a frequency band wider than the optimized range.

Across all test cases, the differences between conducted and radiated excitation errors are minimal across the considered frequencies. It is important to note that the conducted measurements capture only the non-idealities of the BFUs, which exhibit slight deviations from ideal flat amplitude and phase responses. In contrast, the field expansion method accounts for additional sources of excitation error, such as unwanted active impedance effects, which may cause the realized coefficients to diverge from both the excitation values commanded to the BFN, and those verified via conducted measurements.

The strong agreement between the two methods confirms the robustness of the PWG design and its implementation, and validates the accuracy of the field expansion method for this type of analysis. Furthermore, when correlating this excitation error analysis with the achieved PWG performance, it can be concluded that excitation deviations of this magnitude are not critical, and do not compromise the desired system performance.

VI. CONCLUSIONS

The presented work demonstrates the successful implementation and validation of a PWG for low frequency antenna measurement applications. Through both conducted and radiated measurements, excitation errors were thoroughly analyzed using simple VNA-based characterization and a field expansion method. The comparison revealed excellent agreement between the two approaches, confirming the reliability of the programmable beam forming unit, as well as the integrity of the whole BFN. Excitation deviations were found to be minimal and well within acceptable limits for PWG applications, with no significant impact from coupling, active impedance variations, or leakage. These results validate the robustness of the system design and confirm that the achieved excitation accuracy is sufficient to meet the performance requirements of the PWG. Overall, the study highlights the effectiveness of the calibration and optimization strategies employed, and supports the use of the field expansion method as a powerful tool for array excitation analysis.

REFERENCES

[1] IEEE Std 149-2021 “IEEE Recommended Practice for Antenna Measurements”

[2] IEEE Std 1720-2012 “Recommended Practice for Near-Field Antenna Measurements”

[3] F. Scattone *et al*., "Design of Dual Polarised Wide Band Plane Wave Generator for Direct Far-Field Testing," *2019 13th European Conference on Antennas and Propagation (EuCAP)*, Krakow, Poland, 2019

[4] F. Scattone, D. Sekuljica, A. Giacomini, F. Saccardi, A. Scannavini, E. Kaverine, S. Anwar , N. Gross, P. O Iversen, L. J. Foged "Preliminary Assesment of Millimeter Wave Plane Wave Generator For 5G Device Testing"EuCAP 2021, 22-26 March 2021, Düsseldorf, Germany

[5] V. Schirosi *et al*., "Accurate Antenna Characterisation at VHF/UHF Frequencies with Plane Wave Generator Systems," *2023 Antenna Measurement Techniques Association Symposium (AMTA)*, Renton, WA, USA, 2023, pp. 1-6, doi: 10.23919/AMTA58553.2023.10293477.

[6] F. Saccardi *et al*., "Uncertainty of a VHF CubeSat Measurement based on the Synthetic Probe Array Technique," *2023 17th European Conference on Antennas and Propagation (EuCAP)*, Florence, Italy, 2023, pp. 1-5, doi: 10.23919/EuCAP57121.2023.10133319.

[7] F. Saccardi, A. Giacomini, V. Schirosi, L.J. Foged, N. Gross, S. Anwar, E. Kaverine, E. Szpindor, T. McKeown “Synthesis and Validation of Wideband Excitation Coefficients in Plane Wave Generator Systems” EuCAP 2025, Stockholm, Sweden

[8] K. MacReynolds *et al*., “Phased Array Testing and Diagnostics Using Planar Near-Field Scanning”, *AMTA 1992,* Columbus, OH, 8-13, Oct. 1992.

[9] H. M. Aumann and F. G. Willwerth, “Phased array calibrations using measured element patterns,” in International Symposium on Antennas and Propagation, (Long Beach, California), pp. 918–921, IEEE, June 1995.